Geophysical Research Letters

RESEARCH LETTER
10.1029/2025GL116372

Non-Linear and Distinct Responses of Temperature and Precipitation to Volcanic Eruptions With Stratospheric Sulfur Injection From 5 to 160 Tg

Dana Raiter[1,2], **Zachary McGraw**[3,4], **and Lorenzo M. Polvani**[1,2,3]

[1]Department of Earth and Environmental Sciences, Columbia University, New York, NY, USA, [2]Lamont-Doherty Earth Observatory, Columbia University, Palisades, NY, USA, [3]Department of Applied Physics and Applied Mathematics, Columbia University, New York, NY, USA, [4]NASA Goddard Institute for Space Studies, New York, NY, USA

Key Points:

- The simulated climate response to eruptions becomes progressively non-linear as injected sulfur mass is increased from 5 to 160 TgS
- The surface temperature response saturates to about 1° of cooling beyond 40 TgS, but the precipitation keeps decreasing up to 160 TgS
- The mechanisms driving the precipitation response differ between weak and strong volcanic eruptions and this explains its lack of saturation

Supporting Information:

Supporting Information may be found in the online version of this article.

Correspondence to:

D. Raiter,
dana.raiter@columbia.edu

Citation:

Raiter, D., McGraw, Z., & Polvani, L. M. (2025). Non-linear and distinct responses of temperature and precipitation to volcanic eruptions with stratospheric sulfur injection from 5 to 160 Tg. *Geophysical Research Letters*, *52*, e2025GL116372. https://doi.org/10.1029/2025GL116372

Received 4 APR 2025
Accepted 6 OCT 2025

Abstract Much previous modeling work on the climate response to volcanic eruptions has focused on specific past events. Here, we explore the climate response over a whole range of amplitudes covering (and exceeding) all events of the last six millennia, by simulating eruptions with 5, 10, 20, 40, 80, and 160 Tg of stratospheric injected sulfur. Our simulations show a strongly non-linear relationship between eruption magnitude and climate response, with temperature and precipitation responding differently. Global mean surface cooling saturates at 40 TgS, whereas precipitation decreases all the way to 160 TgS. We also find that the precipitation responds and recovers faster than the temperature, especially for the larger events. Our findings imply that a severe reduction in precipitation, rather than a dramatic surface cooling, might be the most important climatic impact associated with very large eruptions.

Plain Language Summary Records from past climates suggest that volcanic eruptions can cool the Earth and affect rainfall patterns. Most previous studies have focused on individual past eruptions. But, in this study, we use climate model simulations to look at how the Earth responds to a wider range of volcanic eruption sizes by simulating progressively larger amounts of sulfur injections into the stratosphere. Our wide range of eruptions covers all events that occurred in the last 6,000 years. We find that the relationship between eruption size and climate effects is not straightforward. Cooling of the Earth's surface stops increasing after a certain eruption size (40 Tg of injected sulfur), but the global rainfall continues to decrease all the way to our largest eruption size (up to 160 Tg of injected sulfur). We also find that rainfall recovers faster than temperature after an eruption. This suggests that for very large volcanic eruptions, the most significant impact might be severe reductions in rainfall, rather than extreme surface cooling.

1. Introduction

Historical and paleoclimatic records have unveiled global impacts of volcanic eruptions on Earth's climate system (Lamb & Sawyer, 1970; Robock, 2000; Timmreck, 2012). It is well known that large eruptions cause a global cooling for several years following the events (e.g., Robock & Mao, 1995; Tejedor et al., 2021a). Additionally, volcanic impacts on precipitation have been suggested, in models and observations, both globally and regionally (e.g., Gao & Gao, 2024; Gillett et al., 2004; Iles & Hegerl, 2014; Iles et al., 2013; Tejedor et al., 2021b; Zuo et al., 2019). The associated effects on human societies are of broad interest. Recent work suggests that severe hydroclimate risks are spatially limited, even after the largest eruptions of the historical period, yet highlights that volcanic risks warrent carful further investigation (McGraw & Polvani, 2025).

While interest in post-eruption climates largely arises from purported impacts on human populations of the past (e.g., Ambrose, 1998; McConnell et al., 2020; Stommel & Stommel, 1979), the only well-observed climatically significant eruption events have been smaller than those in popular theories of past climates. Further, given the rarity of large eruptions, insights on post-eruption climates have largely been established by jointly examining historical eruption events of different magnitude, in what is known as a "superposed epoch analysis," whereby all the events are averaged together to best bring out the volcanic signal. This method prevents one from determining how the climatic impacts scale with the magnitude of the eruption, that is, with the amount of sulfur injected into the stratosphere.

Fortuitously, climate models can be used to determine this scaling. Performing a sufficiently large ensemble of simulations for a given eruption magnitude we can separate the volcanic signal from internal variability. And spanning a broad range of injected sulfur masses allows us to determine the scaling. Two recent studies have taken this approach with respect to the specific question of whether volcanic aerosols cause winter warming over Eurasia (Azoulay et al., 2021; DallaSanta & Polvani, 2022). More recently Timmreck et al. (2024) used this approach to examine the global climate responses to eruptions with injected sulfur masses spanning from 2.5 to 40 TgS with the MPI-ESM model. The key finding of that study is that both the temperature and precipitation responses scale linearly with the injected sulfur mass. In contrast, with smaller ensembles of a different model, but over a broader range from 9 to 1,000 TgS, McGraw et al. (2024) reported that post-eruption cooling is highly non-linear, and saturates somewhere between 50 and 150 TgS.

Building on this work, we here analyze large ensembles of simulations that capture (and exceed) the entire magnitude range of the last six millennia, by progressively doubling the injected sulfur masses from 5 to 160 TgS. The largest event of the last 6,000 years is the 1257 CE eruption of Mt. Samalas, with an estimated sulfur injection of nearly 60 TgS (Sigl et al., 2022; Toohey & Sigl, 2017) and has been linked to widespread famines in Europe and pestilence in the Middle East (Campbell, 2017; Stothers, 1984). Our largest assessed eruption is 2.5 times larger than this event, placing it within the plausible mass range of volcanic super-eruptions (Oppenheimer, 2002). As shown below, our analysis confirms the existence of a linear response up to 20 TgS, but reveals a breakdown of the linear response for 40 TgS and above. In addition we show that while the temperature response saturates above that level, the precipitation response does not, as the controlling mechanisms change from the weak to the strong eruptions, as detailed below.

2. Methods

The model used for our simulations is the Goddard Institute for Space Studies (GISS) ModelE2.2, a "high-top" version of the NASA GISS ModelE earth system model, with well-resolved stratospheric climate dynamics (Orbe et al., 2020). The volcanic aerosols in this model are prescribed by reading in aerosol extinction and size parameters constructed with the Easy Volcanic Aerosol (EVA) forcing generator (Toohey et al., 2016). The advantage of using EVA is that identical volcanic aerosols can be prescribed across different models, reducing one source of uncertainty. The key parameter controlling the eruption magnitude is the mass of sulfur injected into the stratosphere: we choose injection masses of 5, 10, 20, 40, 80, and 160 TgS to cover the entire range of amplitudes of eruptions since the mid-Holocene (see Figure 7a of Sigl et al. (2022)). For each magnitude, we analyze 20 ensemble members to separate the forced response from internal variability. The vertical and latitudinal distributions of the EVA aerosols used in our model can be found in Figure 1 of DallaSanta and Polvani (2022), who originally performed these simulations.

To quantify the climatic impact of these volcanic eruptions, we compare the temperature and precipitation fields following each event to those of a long control run with no volcanic aerosols. Each forced simulation is paired to the control run, matching the same years and same initial conditions, to account for low-frequency natural variability (DallaSanta & Polvani, 2022). For each simulation, then, the response of any variable is defined as the difference (Δ hereafter) between the forced simulation and the paired control run. Averaging over all 20 members for each forcing amplitude yields what we refer to as the "forced response" caused by the eruption (Deser et al., 2012).

To delve deeper into the mechanism of the precipitation response, we separate the response caused by the colder sea surface temperature (SST), known as the "slow" response, from the one caused by the SST-independent atmospheric adjustments, known as the "fast" response. This separation is widely used to analyze the precipitation response to abrupt CO_2 forcing (e.g., Andrews et al., 2010). It was recently extended to the study of the response to volcanic eruptions by McGraw and Polvani (2024), who found that the global post-eruption reduction in precipitation can be separated into a slow component driven by volcanic cooling of the surface that lasts for several years, and a fast 1–2 year response triggered by volcanic aerosols absorbing and emitting longwave radiation. To compute these two components one needs to perform—for each simulation—a companion run with volcanic aerosols prescribed in the atmospheric model alone, and with the SST and sea-ice prescribed from the corresponding years in the control runs with no volcanic aerosols. The difference in precipitation between the control run and the prescribed-SST run with volcanic aerosols gives the SST-independent precipitation response to the eruption (the fast response).

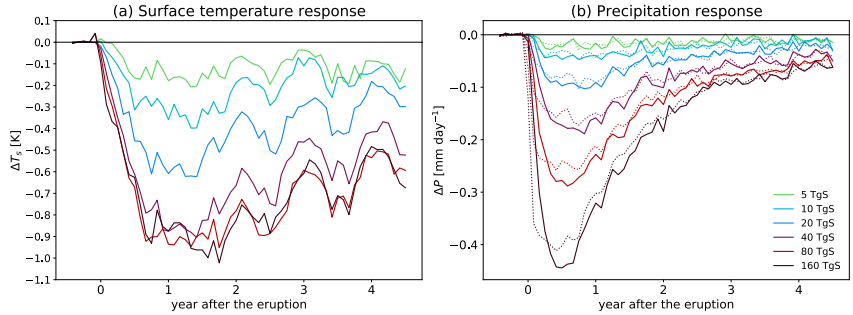

Figure 1. Time series of global mean (a) surface temperature and (b) precipitation response, averaged over the 20-member ensembles, for eruptions of 5–160 TgS amplitude, from the fully coupled model simulations. The dotted line in panel (b) shows atmospheric energy flux (the right-hand side of Equation 2).

3. Results

3.1. Post-Eruption Temperature and Precipitation Responses

The global mean surface temperature and precipitation responses to volcanic eruptions, with sulfur emissions ranging from 5 to 160 TgS, are shown in Figure 1. The time series for temperature (Figure 1a) reveal a pronounced cooling effect following each eruption, with larger eruptions causing stronger cooling. More interesting, however, a saturation effect is apparent for the three largest injection masses: note how 40, 80, and 160 TgS injection yield very similar global cooling. As for the recovery time, we see that even for the smaller injections, the forced response is non-zero over the first four post-eruption years (Figure 1a). As shown in Figure S1 in Supporting Information S1, it takes 7–10 years for the forced response (solid colored lines in each panel) to vanish, depending on amplitude.

Turning now to global mean precipitation response (Figure 1b), we notice several differences. First, unlike temperature, the reduction in precipitation shows no sign of saturation past 40 TgS, with large decreases all the way to 160 TgS. Second, the recovery rate for precipitation is not the same as for temperature. Notice how the very large precipitation response decreases rapidly after the first year, unlike the temperature response. And on longer time scales (Figure S1 in Supporting Information S1), the forced response in precipitation is not a linear function of time, unlike the temperature response.

It is most important to place these forced responses in the context of internal variability, which is quite large, even for globally averaged quantities. In each panel of Figure S1 in Supporting Information S1, the two black dotted horizontal lines represent the $\pm 2\sigma$ (standard deviation) of the control run, while the shaded colored area indicates the spread across each 20-member ensemble. For simplicity, we will here consider the forced response to be significant if it lies outside the $\pm 2\sigma$ range. In our simulations, neither temperature nor precipitation responses are significant for the smallest eruptions (5 TgS). Even for 10 TgS eruptions, a mass of injected sulfur roughly corresponding the one of the 1991 Pinatubo eruption, the temperature response is not significant; and, while the ensemble-mean precipitation response exceeds the 2σ line in years 1 and 2 (Figure S1d in Supporting Information S1), the time series of individual members (not shown here) is very noisy, and the ensemble spread includes the abscissa. This supports the finding of Timmreck et al. (2024), who reported that 20 TgS is the threshold beyond which the response exceeds the range of internal variability.

The substantial differences between the post-eruption temperature and precipitation, particularly the clear saturation of the temperature but not the precipitation response (Figure 1), suggest that we need to more carefully examine the non-linear dependence of these responses on the magnitude of the eruption. This is done in Figures 2a and 2b where we present the surface temperature and precipitation responses, here averaged over the first 4 years following an eruption, and as a function of injected sulfur mass. Note that the uncertainty (not shown) was found to be very small. The solid line shows the forced response and the gray line shows the linear approximation, calculated using the 20 TgS eruptions as a reference (extrapolating the slope from 5 to 20 TgS, assuming linearity). It is clear that both surface temperature and precipitation respond linearly between 5 and 20 TgS, but for 40 TgS and above, the response increasingly deviates from the linear curve.

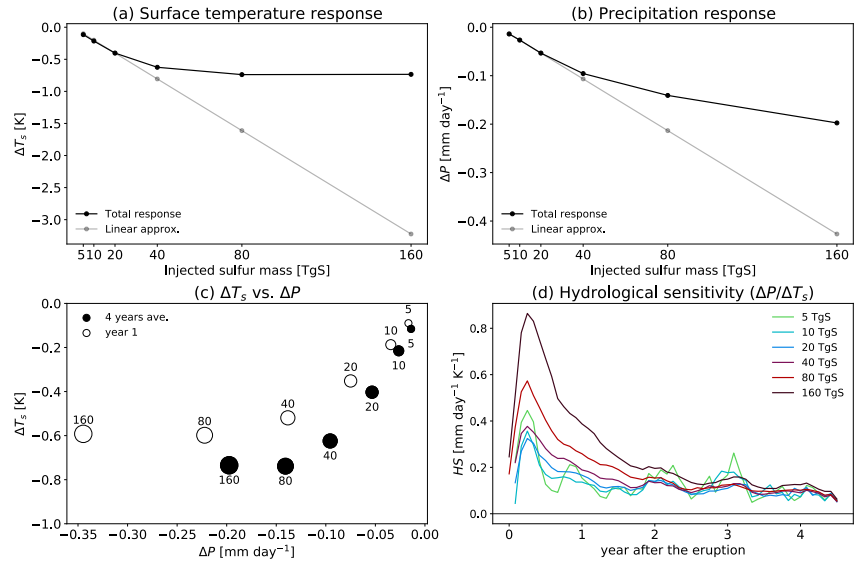

Figure 2. Ensemble mean, global mean (a) surface temperature and (b) precipitation response, averaged over the first 4 years after the eruptions; solid lines show the simulated response, and gray lines show the linear approximation based on the 20 TgS case. (c) Global mean surface temperature and precipitation responses, averaged over the first 4 years (black filled dots) and the first year (empty dots) after the eruption; the size of the dot represents the magnitude of the eruption, from smallest (5 TgS) to largest size (160 TgS). (d) Time series of the apparent hydrological sensitivity η_a, with a 3-month smoothing filter.

Although both precipitation and temperature respond non-linearly for large enough eruptions, the non-linearity manifests itself differently. This difference is illustrated in Figure 2c, where the temperature response is plotted against the precipitation response, each point corresponding to a different eruption magnitude. Averaging over the first 4 years following the eruption (solid dots), the temperature and precipitation responses appear linearly related between up to 20 TgS. However, for eruptions exceeding 40 TgS, the temperature response saturates while the precipitation response continues to increase, breaking the linear relationship. This behavior is robust to the averaging interval, and can also be seen using only the first post-eruption year (empty dots).

When considering the climate response to increasing carbon dioxide (CO_2), it is customary to express the relationship between precipitation and temperature responses as the transient "apparent hydrological sensitivity" η_a, calculated as the ratio of the response in precipitation ΔP to the response in temperature ΔT (Fläschner et al., 2016). The time series of η_a, for each eruption magnitude, are shown Figure 2d, with a 3-month smoothing. The ensemble mean value of η_a, averaged over the first post-eruption year, is given in Table S1 in Supporting Information S1. Note that η_a is very similar for eruptions with 5 and 10 TgS, but becomes progressively larger for larger eruptions. It is interesting to contrast this behavior with the one under abrupt CO_2 forcing, where η_a remains very nearly constant over a huge range of CO_2 increases (Bonan et al., 2024; Raiter et al., 2023).

3.2. Controlling Mechanisms of Temperature and Precipitation Changes

To dig deeper into the reason for the non-linear behavior of the response with forcing amplitude, we now examine the net top-of-atmosphere (TOA) energy fluxes (F_{TOA}), and their relationship to temperature changes in response to volcanic eruptions. In the simplest case, one would imagine that the saturation of the cooling response for the largest eruptions is a simple consequence of the saturation of the effective radiative forcing ΔF_{TOA}, with feedbacks playing a minor role. That forcing is usually decomposed as follows:

$$\Delta F_{\mathrm{TOA}} = \Delta F_{\mathrm{TOA,IRF}} + \Delta F_{\mathrm{TOA,RA}} \quad (1)$$

where $\Delta F_{\mathrm{TOA,IRF}}$ is the instantaneous radiative forcing due to the presence of the volcanic aerosols, and $\Delta F_{\mathrm{TOA,RA}}$ represents the rapid adjustments, that is, the SST-independent atmosphere changes caused by the eruption that affect radiative forcing (Sherwood et al., 2015). Both of these are computed from the difference in F_{TOA} between

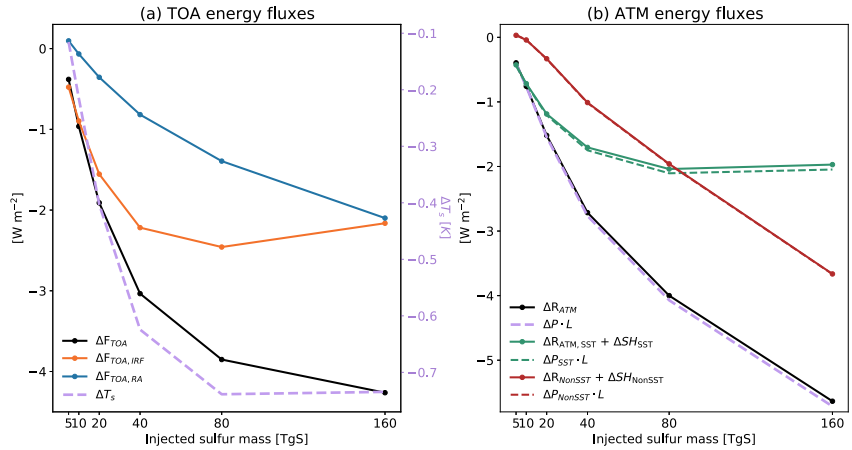

Figure 3. (a) Radiative forcing and (b) atmospheric energy fluxes, averaged over the first 4 years after a volcanic eruption. In panel (a), the effect of radiative forcing (black) is decomposed into instantaneous forcing (orange) and the rapid adjustments (blue), see Equation 1; dashed purple line shows the surface temperature response (note right side axis). In panel (b), the total energy flux (the right-hand side of Equation 3) is decomposed into the sea surface temperature (SST)-mediated part (red, the first term on the right-hand side of Equation 5) and the SST-independent part (green, the second term on the right hand side of Equation 5), ΔR terms are multiplied by (−1); the corresponding dashed lines show the actual precipitation from the model output, multiplied by L.

the simulations with volcanic aerosols present and the control simulation: The IRF is calculated in all simulations using a double radiation call—with and without the volcanic aerosols—and we show the version in the fixed-SST simulations. The RA is calculated as the difference between ΔF_{TOA} and the IRF.

First, as seen in Figure 3a, ΔT_s (dashed purple) roughly tracks ΔF_{TOA} (solid black) indicating that the saturation of the temperature response roughly follows from the saturation of the total radiative forcing at TOA (note that we are not computing radiative feedbacks or ocean heat uptake). Second, from the decomposition in Equation 1 above, it is clear that the instantaneous forcing (orange) dominates over rapid adjustments (blue) for all eruption amplitudes up to 160 TgS. And, more importantly, it is the instantaneous forcing that saturates, and actually starts decreasing in magnitude from 80 to 160 TgS. As explained in McGraw et al. (2024), this is due to the increasing aerosol size for eruptions larger than 20 TgS (explicitly represented in EVA); this dependence of the radiative forcing on aerosols size is long established (Lacis et al., 1992; Timmreck et al., 2009). In contrast, the radiative effect from rapid adjustments is negligible for the smallest eruptions, and grows monotonically as the eruption size increases. Interestingly, for 160 TgS eruptions, the contributions from $\Delta F_{\mathrm{TOA,IRF}}$ and $\Delta F_{\mathrm{TOA,RA}}$ are nearly equal, suggesting that rapid adjustments are important after large eruptions, and could even be the dominant driver of cooling for super-eruptions.

Turning now to the global mean precipitation P, we adopt standard energy balance analysis (O'Gorman et al., 2011):

$$L\Delta P \approx -\Delta R_{\mathrm{ATM}} - \Delta \mathrm{SH}, \tag{2}$$

where L is the latent heat of condensation and ΔP is the precipitation response. The term ΔR_{ATM} is the change (with respect to the control run) in column-integrated atmospheric radiative flux (known as the "radiative cooling" term); recall that ΔR_{ATM} is calculated as the change at the top of the atmosphere minus the change at the surface. Finally, ΔSH is the change in sensible heat flux.

The accuracy of the energy balance analysis can be seen in Figure 1b. See how closely the dotted lines, representing ΔP as computed from Equation 2, track the actual the precipitation response (solid lines), even for the very largest eruptions. Such accuracy was demonstrated by McGraw and Polvani (2024) for 20 TgS eruptions, and we here show that this approximation remains valid across a wide range of eruption magnitudes.

With this in hand, we next decompose each term on the right Equation 2 into an SST-mediated and an SST-independent component. The latter are obtained from the runs with volcanic aerosols but fixed SST. The SST-

mediated components are simply the difference between the fully coupled and the SST-independent components. Specifically:

$$L\Delta P \approx -\Delta R_{\mathrm{ATM}} - \Delta \mathrm{SH}, \tag{3}$$

$$\approx -(\Delta R_{\mathrm{ATM,SST}} + \Delta R_{\mathrm{ATM,nonSST}}) - (\Delta \mathrm{SH}_{\mathrm{SST}} + \Delta \mathrm{SH}_{\mathrm{nonSST}}) \tag{4}$$

$$\approx -(\Delta R_{\mathrm{ATM,SST}} + \Delta \mathrm{SH}_{\mathrm{SST}}) - (\Delta R_{\mathrm{ATM,nonSST}} + \Delta \mathrm{SH}_{\mathrm{nonSST}}) \tag{5}$$

$$\approx L\Delta P_{\mathrm{SST}} + L\Delta P_{\mathrm{nonSST}} \tag{6}$$

where the subscript "SST" denotes the SST-mediated component, and the subscript "nonSST" the SST-independent component. All the terms in Equations 3, 5, and 6 are shown in Figure 3b. Note that the black lines are, by construction, the sums to the corresponding red and green lines.

For the smaller eruptions, the precipitation response (black lines) is dominated by the SST-mediated component (green lines), indicating that surface cooling is the main driver of the reduced precipitation. However, as the eruption size increases, the SST-independent component (red lines) becomes increasingly significant. For an 80 TgS eruption, both components contribute almost equally to the reduction in precipitation, and for a 160 TgS eruption, the SST-independent component becomes dominant. This reversal in the relative importance of the components highlights a change in the mechanisms driving precipitation responses, and reveals how the non-linearity emerges from the weak to the large eruptions. Note that the solid and dashed lines are nearly identical, indicating that the global mean precipitation response is strongly constrained by the energy balance.

Finally, we again emphasize that the precipitation response does not saturate for very large eruptions, unlike the temperature response. The decomposition in Equation 6 allows us to understand why. As seen in Figure 3b, the SST-mediated component of ΔP does in fact saturate (green), as one would expect from the fact that the SST cooling saturates beyond 40 TgS. But the SST-independent component of ΔP continues to increase in magnitude all the way to 160 TgS. Hence, the continued global drying as eruption magnitude is increased is caused by the direct radiative effects of the aerosols. This reduction is driven by the aerosols absorbing and emitting longwave radiation (McGraw & Polvani, 2024), which produces a stratosphere that emits enhanced radiative flux downward into the underlying troposphere, where it alters cloud and convective processes and in turn inhibits precipitation. The fact that the global mean precipitation response does not scale with the global mean surface temperature response for large eruptions is one of the key findings of our study.

3.3. Regional Analysis of the Responses

Finally, to go beyond global mean values, in Figure 4 we present maps of temperature and precipitation responses, averaged over the first four post-eruption years. Let us start by examining the temperature response, shown in the left column for the 20, 40, and 160 TgS cases. Note that the responses for 40 and 160 TgS have been divided by 2 and 8, to bring out the non-linear character of the response. As one can see, the colors are much more muted for 160 TgS compared to 20 TgS; nonetheless, the area with a statistically significant response is larger for 160 TgS (for simplicity, we here define the response to be significant if more than 80% of the ensemble members agree on the sign; using a more common *t*-test with 95% confidence level yields a nearly identical figure). Unsurprisingly, for all eruption magnitudes, the surface temperature response is a cooling nearly everywhere. However, the Southern Ocean stands out as a region lacking a statistically significant response (notably the Atlantic and Indian sectors), even for largest eruptions; this is likely related to the transient nature of the forcing, and the ability of the Southern Ocean circulation to advect the anomaly away from the surface (J. Marshall et al., 2015).

Turning now to precipitation, let us consider the total response shown in the second column (Figures 4b, 4f, and 4j). Note first the very large spatial variance, with both drying and large wetting regions present. This implies that the global mean value results from large cancellation from these different regions, and hence may not be representative of regional responses. Second, and more importantly, we emphasize that the regional response is statistically insignificant almost everywhere for a 20 TgS eruption, which is twice the size of the 1991 Pinatubo event. And even for a 40 TgS eruption, which is larger than all eruptions of the last several millennia except the single 1257 Samalas event, the regions with significance are confined to drying bands in the mid-latitudes. However, unlike Timmreck et al. (2024), the significant precipitation responses are not confined to the tropics and

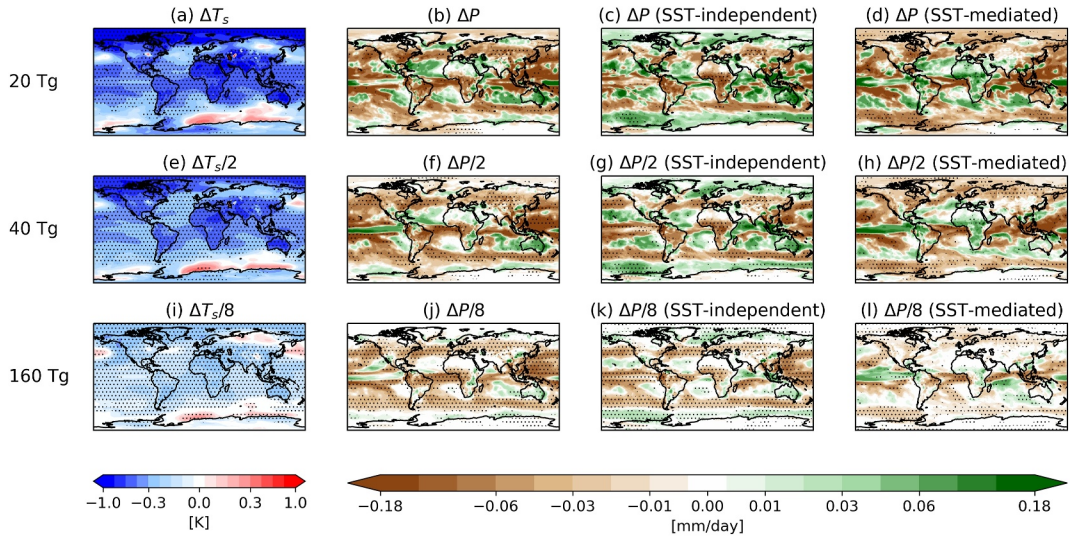

Figure 4. Scaled maps of ensemble mean surface temperature (first column) and precipitation (second column) response, averaged over the first 4 years after the eruption, for 20, 40, and 160 TgS eruptions. The sea surface temperature (SST)-mediated and SST-independent components of the precipitation response are in the 3rd and 4th column. Stippling indicates regions where more than 80% of the ensemble members agree on the sign.

subtropics for the very large eruptions. Third, as for temperature, one can see the non-linearity in the precipitation response as the colors are more muted for the scaled 160 TgS eruptions than for 20 TgS.

Fourth, and finally, we highlight large regional cancellation between the SST-mediated and SST-independent components (contrast the third and fourth column). For instance, consider the response to a 20 TgS eruption over Africa. The SST-mediated component is a wetting of that continent (opposite to what one might naively expect to accompany a global cooling), whereas the SST-independent component is a drying. Surprisingly, it is the latter component that dominates the total signal, unlike for the global mean precipitation response, which is controlled by the SST-mediated component (see Figure 3b). And, to add more complexity, for the very largest forcing the response in most regions is clearly dominated by the SST-independent component (note the similarity between Figure 4j and Figure 4k). Hence, the regional responses are complex, and not necessarily represented by the global mean response.

4. Summary and Discussions

Our systematic exploration of the climate response to volcanic eruptions over a broad range of magnitudes spanning all the major events since the mid-Holocene has yielded several new findings. First, our simulations confirm the fundamentally non-linear character of the response for stratospheric sulfur injections larger than 40 TgS, not simply in global mean surface cooling (as reported by McGraw et al. (2024)) but also in precipitation. Second, we have found that the non-linear response differs markedly between temperature and precipitation: the former actually saturates, so that 40, 80, and 160 TgS eruptions cause basically identical global cooling, whereas precipitation continues to decrease all the way to 160 TgS, albeit at a slower than linear rate. Third, we have shown that while SST dominates the precipitation response for eruptions up to 40 TgS, the direct radiative aerosol-induced warming of the lower stratosphere dominates the precipitation response at 160 TgS. As a consequence, for the larger eruptions the time scale of the precipitation response is shorter than the time scale of the temperature response.

Our findings give new insights on potential risks associated with very large eruptions. Unlike surface temperature, the precipitation response does not saturate with increasing eruption mass, and this could pose the greatest global-scale threat after super-eruptions and other very large volcanic events. Therefore, although there is evidence that temperature effects of super-eruptions are limited (McGraw et al., 2024; Timmreck et al., 2009), our findings suggest a need to probe the existence of exceptional post-eruption precipitation, and specifically in the first 1–2 years after these extreme events. While the precipitation impacts of large holocene eruptions have been

demonstrated to pose limited threats (McGraw & Polvani, 2025), our new finding gives a basis for potentially far strongerthreats rom super-eruptions. We note however, that models disagree on the magnitude of fast precipitation responses to stratospheric aerosols (Ferraro & Griffiths, 2016) and hence, further evaluation is warrented.

While our findings provide valuable new insights into the climate response to volcanic eruptions, we acknowledge several uncertainties that we hope to address in future research. First we emphasize that the poorly constrained aerosol size after large eruptions drives considerable uncertainty in the volcanic forcing, which in turn affects the temperature and precipitation responses (McGraw et al., 2024; McGraw & Polvani, 2025). Additionally, injection height, location, and season are also potential sources of uncertainty, as different injection scenarios can lead to varying climate responses (L. Marshall et al., 2019). Finally, we recognize that our study relies on a single model (GISS ModelE2.2). These caveats highlight the need for multi-model and large ensemble approaches to robustly quantify climate responses to volcanic eruptions and ensure more reliable uncertainty estimates.

Conflict of Interest

The authors declare no conflicts of interest relevant to this study.

Data Availability Statement

ModelE source code is available online (https://www.giss.nasa.gov/tools/modelE/) and simulation output used here is on a Zenodo archive (Raiter et al., 2025).

Acknowledgments
This work was funded by awards 2335763 and 2303352 from the US National Science Foundation to Columbia University.

References

Ambrose, S. H. (1998). Late Pleistocene human population bottlenecks, volcanic winter, and differentiation of modern humans. *Journal of Human Evolution*, *34*(6), 623–651. https://doi.org/10.1006/jhev.1998.0219

Andrews, T., Forster, P. M., Boucher, O., Bellouin, N., & Jones, A. (2010). Precipitation, radiative forcing and global temperature change. *Geophysical Research Letters*, *37*(14), L14701. https://doi.org/10.1029/2010gl043991

Azoulay, A., Schmidt, H., & Timmreck, C. (2021). The arctic polar vortex response to volcanic forcing of different strengths. *Journal of Geophysical Research: Atmospheres*, *126*(11), e2020JD034450. https://doi.org/10.1029/2020JD034450

Bonan, D. B., Schneider, T., & Zhu, J. (2024). Precipitation over a wide range of climates simulated with comprehensive GCMs. *Geophysical Research Letters*, *51*(16), e2024GL109892. https://doi.org/10.1029/2024gl109892

Campbell, B. M. S. (2017). Global climates, the 1257 mega-eruption of Samalas volcano, Indonesia, and the English food crisis of 1258. *Transactions of the Royal Historical Society*, *27*, 87–121. https://doi.org/10.1017/s0080440117000056

DallaSanta, K., & Polvani, L. M. (2022). Volcanic stratospheric injections up to 160 Tg(s) yield a Eurasian winter warming indistinguishable from internal variability. *Atmospheric Chemistry and Physics*, *22*(13), 8843–8862. https://doi.org/10.5194/acp-22-8843-2022

Deser, C., Phillips, A., Bourdette, V., & Teng, H. (2012). Uncertainty in climate change projections: The role of internal variability. *Climate Dynamics*, *38*(3–4), 527–546. https://doi.org/10.1007/s00382-010-0977-x

Ferraro, A. J., & Griffiths, H. G. (2016). Quantifying the temperature-independent effect of stratospheric aerosol geoengineering on global-mean precipitation in a multi-model ensemble. *Environmental Research Letters*, *11*(3), 034012. https://doi.org/10.1088/1748-9326/11/3/034012

Fläschner, D., Mauritsen, T., & Stevens, B. (2016). Understanding the intermodel spread in global-mean hydrological sensitivity. *Journal of Climate*, *29*(2), 801–817. https://doi.org/10.1175/jcli-d-15-0351.1

Gao, Y., & Gao, C. (2024). Dwindling effective radiative forcing of large volcanic eruption: The compensation role of ocean latent heat flux. *Geophysical Research Letters*, *51*(15), e2024GL109885. https://doi.org/10.1029/2024gl109885

Gillett, N., Weaver, A., Zwiers, F., & Wehner, M. (2004). Detection of volcanic influence on global precipitation. *Geophysical Research Letters*, *31*(12), L12217. https://doi.org/10.1029/2004gl020044

Iles, C. E., & Hegerl, G. C. (2014). The global precipitation response to volcanic eruptions in the CMIP5 models. *Environmental Research Letters*, *9*(10), 104012. https://doi.org/10.1088/1748-9326/9/10/104012

Iles, C. E., Hegerl, G. C., Schurer, A. P., & Zhang, X. (2013). The effect of volcanic eruptions on global precipitation. *Journal of Geophysical Research: Atmospheres*, *118*(16), 8770–8786. https://doi.org/10.1002/jgrd.50678

Lacis, A., Hansen, J., & Sato, M. (1992). Climate forcing by stratospheric aerosols. *Geophysical Research Letters*, *19*(15), 1607–1610. https://doi.org/10.1029/92gl01620

Lamb, H. H., & Sawyer, J. S. (1970). Volcanic dust in the atmosphere; with a chronology and assessment of its meteorological significance. *Philosophical Transactions of the Royal Society of London - Series A: Mathematical and Physical Sciences*, *266*(1178), 425–533. https://doi.org/10.1098/rsta.1970.0010

Marshall, J., Scott, J. R., Armour, K. C., Campin, J.-M., Kelley, M., & Romanou, A. (2015). The ocean's role in the transient response of climate to abrupt greenhouse gas forcing. *Climate Dynamics*, *44*(7–8), 2287–2299. https://doi.org/10.1007/s00382-014-2308-0

Marshall, L., Johnson, J. S., Mann, G. W., Lee, L., Dhomse, S. S., Regayre, L., et al. (2019). Exploring how eruption source parameters affect volcanic radiative forcing using statistical emulation. *Journal of Geophysical Research: Atmospheres*, *124*(2), 964–985. https://doi.org/10.1029/2018JD028675

McConnell, J. R., Sigl, M., Plunkett, G., Burke, A., Kim, W. M., Raible, C. C., et al. (2020). Extreme climate after massive eruption of Alaska's Okmok volcano in 43 BCE and effects on the late roman republic and Ptolemaic Kingdom. *Proceedings of the National Academy of Sciences of the United States of America*, *117*(27), 15443–15449. https://doi.org/10.1073/pnas.2002722117

McGraw, Z., DallaSanta, K., Polvani, L. M., Tsigaridis, K., Orbe, C., & Bauer, S. E. (2024). Severe global cooling after volcanic super-eruptions? The answer hinges on unknown aerosol size. *Journal of Climate*, *37*(4), 1449–1464. https://doi.org/10.1175/JCLI-D-23-0116.1

McGraw, Z., & Polvani, L. M. (2024). How volcanic aerosols globally inhibit precipitation. *Geophysical Research Letters*, *51*(13), e2023GL107930. https://doi.org/10.1029/2023gl107930

McGraw, Z., & Polvani, L. M. (2025). Do climate models support claims of volcanic global catastrophes? *Geophysical Research Letters*, *52*(18), e2025GL117611. https://doi.org/10.1029/2025GL117611

O'Gorman, P. A., Allan, R. P., Byrne, M. P., & Previdi, M. (2011). Energetic constraints on precipitation under climate change. *Surveys in Geophysics*, *33*(3–4), 585–608. https://doi.org/10.1007/s10712-011-9159-6

Oppenheimer, C. (2002). Limited global change due to the largest known quaternary eruption, Toba 74kyr BP? *Quaternary Science Reviews*, *21*(14–15), 1593–1609. https://doi.org/10.1016/s0277-3791(01)00154-8

Orbe, C., Rind, D., Jonas, J., Nazarenko, L., Faluvegi, G., Murray, L. T., et al. (2020). GISS model e2.2: A climate model optimized for the middle atmosphere—2. Validation of large-scale transport and evaluation of climate response. *Journal of Geophysical Research: Atmospheres*, *125*(24), e2020JD033151. https://doi.org/10.1029/2020JD033151

Raiter, D., McGraw, Z., DallaSanta, K., & Polvani, L. M. (2025). Modele2.2 output used in "non-linear and distinct responses of temperature and precipitation to volcanic eruptions with stratospheric sulfur injection from 5 to 160 Tg" study [Dataset]. *Zenodo*. https://doi.org/10.5281/zenodo.15126907

Raiter, D., Polvani, L. M., Mitevski, I., Pendergrass, A. G., & Orbe, C. (2023). Little change in apparent hydrological sensitivity at large CO_2 forcing. *Geophysical Research Letters*, *50*(18), e2023GL104954. https://doi.org/10.1029/2023GL104954

Robock, A. (2000). Volcanic eruptions and climate. *Reviews of Geophysics*, *38*(2), 191–219. https://doi.org/10.1029/1998RG000054

Robock, A., & Mao, J. (1995). The volcanic signal in surface temperature observations. *Journal of Climate*, *8*(5), 1086–1103. https://doi.org/10.1175/1520-0442(1995)008<1086:tvsist>2.0.co;2

Sherwood, S. C., Bony, S., Boucher, O., Bretherton, C., Forster, P. M., Gregory, J. M., & Stevens, B. (2015). Adjustments in the forcing-feedback framework for understanding climate change. *Bulletin of the American Meteorological Society*, *96*(2), 217–228. https://doi.org/10.1175/bams-d-13-00167.1

Sigl, M., Toohey, M., McConnell, J. R., Cole-Dai, J., & Severi, M. (2022). Volcanic stratospheric sulfur injections and aerosol optical depth during the Holocene (past 11 500 years) from a bipolar ice-core array. *Earth System Science Data*, *14*(7), 3167–3196. https://doi.org/10.5194/essd-14-3167-2022

Stommel, H., & Stommel, E. (1979). The year without a summer. *Scientific American*, *240*(6), 176–187. Retrieved from http://www.jstor.org/stable/24965226

Stothers, R. B. (1984). The great Tambora eruption in 1815 and its aftermath. *Science*, *224*(4654), 1191–1198. https://doi.org/10.1126/science.224.4654.1191

Tejedor, E., Steiger, N., Smerdon, J. E., Serrano-Notivoli, R., & Vuille, M. (2021a). Global temperature responses to large tropical volcanic eruptions in paleo data assimilation products and climate model simulations over the last millennium. *Paleoceanography and Paleoclimatology*, *36*(4), e2020PA004128. https://doi.org/10.1029/2020PA004128

Tejedor, E., Steiger, N. J., Smerdon, J. E., Serrano-Notivoli, R., & Vuille, M. (2021b). Global hydroclimatic response to tropical volcanic eruptions over the last millennium. *Proceedings of the National Academy of Sciences of the United States of America*, *118*(12), e2019145118. https://doi.org/10.1073/pnas.2019145118

Timmreck, C. (2012). Modeling the climatic effects of large explosive volcanic eruptions. *Wiley Interdisciplinary Reviews: Climate Change*, *3*(6), 545–564. https://doi.org/10.1002/wcc.192

Timmreck, C., Lorenz, S. J., Crowley, T. J., Kinne, S., Raddatz, T. J., Thomas, M. A., & Jungclaus, J. H. (2009). Limited temperature response to the very large ad 1258 volcanic eruption. *Geophysical Research Letters*, *36*(21), L21708. https://doi.org/10.1029/2009gl040083

Timmreck, C., Olonscheck, D., Ballinger, A. P., D'Agostino, R., Fang, S.-W., Schurer, A. P., & Hegerl, G. C. (2024). Linearity of the climate response to increasingly strong tropical volcanic eruptions in a large ensemble framework. *Journal of Climate*, *37*(8), 2455–2470. https://doi.org/10.1175/JCLI-D-23-0408.1

Toohey, M., & Sigl, M. (2017). Volcanic stratospheric sulfur injections and aerosol optical depth from 500 BCE to 1900 CE. *Earth System Science Data*, *9*(2), 809–831. https://doi.org/10.5194/essd-9-809-2017

Toohey, M., Stevens, B., Schmidt, H., & Timmreck, C. (2016). Easy volcanic aerosol (Eva v1.0): An idealized forcing generator for climate simulations. *Geoscientific Model Development*, *9*(11), 4049–4070. https://doi.org/10.5194/gmd-9-4049-2016

Zuo, M., Zhou, T., & Man, W. (2019). Wetter global arid regions driven by volcanic eruptions. *Journal of Geophysical Research: Atmospheres*, *124*(24), 13648–13662. https://doi.org/10.1029/2019jd031171